SGLI

Algorithm Theoretical Basis Document

ATMOSPHERIC CORRECTION ALGORITHM

FOR OCEAN COLOR

Version 2 July 3 2020

Mitsuhiro Toratani,

Kazunori Ogata* and Hajime Fukushima

Tokai University

*JAXA/EORC

Table of Contents

1. Introduction

This ATBD describes the atmospheric correction of ocean color remote sensing for GCOM-C/SGLI.

The purpose of the atmospheric corrections is to retrieve the water-leaving radiance spectrum from the radiance spectrum observed by the satellite. It is necessary to correct for the effects of the atmosphere and sea surface in the radiance observed by the satellite. Atmospheric effects include scattering of gas molecules, scattering of aerosols, absorption of gases and aerosols, as well as sea surface effects, such as sunglint, whitecaps, and bidirectional reflectance distribution.

Atmospheric correction methods for SGLI are based on the SeaWiFS and MODIS atmospheric corrections (Gordon and Wang, 1994) and also the Japanese ocean color satellite ADEOS/OCTS (Fukushima et al.,1998) and ADEOS2/GLI (Toratani et al. al.,2007).

The following items have been updated from Version 1 of the SGLI atmospheric correction.

(1) Updated lookup table for aerosols

The relationship between the aerosol reflectance and the optical thickness of the aerosol was recalculated using radiative transfer simulations. In Ver.1, the upper limit of optical thickness was set at 0.3, but this was not always appropriate. The upper limit of the aerosol optical thickness was reviewed for each aerosol model, and the lookup tables of aerosols was updated.

(2) Change in the aerosol model selection method

In Ver.1, the inter-wavelength ratio (ε) of the single-scattering aerosol reflectance between two wavelengths was used to select the aerosol models. In Ver. 2, the inter-wavelength ratio of aerosol-optical-thickness is used in order to simplify and speed up the processing. The combination of wavelengths used for model selection is twofold, that is either of "673nm & 869nm" and "869nm & 1630 nm" bands. The conditions for switching the combination were changed.

(3) Update of the in-water model

More realistic in-water model (Ahn et al., 2015; Lee et al., 2002) is used for calculating aerosol reflectance in the iterative aerosol correction procedure. The convergence conditions for the iterative calculation were changed accordingly. For the atmospheric correction with 869 nm and 1630 nm, an iterative operation is also introduced.

(4) Calculation method of sunglitter

The method for calculating direct transmittance was changed.

2. Radiative transfer equation for radiance

The top of atmospheric radiance L_T^* observed by satellite sensors is expressed as (Gordon, 1997; Mobley et al., 2016),

$$L_T^* = L_{path}^* + T^*L_G + t^*L_{WC} + t^*L_W \quad [W\ m^{-2}\ \mu m^{-1}\ sr^{-1}], \tag{2.1}$$

where L_{path}^* is the atmospheric radiation composed of the atmospheric scattered light and the sky light specularly reflected at the ocean surface, L_G is the sunglint radiance of the direct beam reflected by sea surface, L_{WC} is the radiance reflected by the whitecap, L_W is water-leaving radiance, respectively. For simplicity, we omit the wavelength λ. Since L_G, L_{WC} and L_W are the radiance at the sea surface, the transmittance of the atmosphere from the sea surface to the satellite should be applied. Expressions T^* and t^* are used for the direct and diffuse transmittance by the atmosphere from the sea surface to the sensor. We consider T^* and t^* to be composed of the following elements.

$$T^* = t^{(O3)}T^{(g)}T^{(M)}T^{(A)}, \tag{2.2}$$
$$t^* = t^{(O3)}t^{(g)}t^{(M)}t^{(A)}. \tag{2.3}$$

In the right-hand side, the superscript O3 indicates absorption of ozone, g indicates absorption by gases other than ozone (such as O2, NO2 and H2O), M indicates scattering of atmospheric molecules, and A indicates extinction of aerosols. Since ozone is predominantly present in the upper atmosphere, its interactions with other elements are negligible. The effect of ozone absorption occurs twice, once when sunlight enters the atmosphere and once when it is emitted. The ozone transmittance is assumed to affect all components of L_T^*, and hence the equation (2.1) can be transformed as follows.

$$\begin{gathered} L_T^* = \left(\frac{L_{path}^*}{t^{(O3)}t_0^{(O3)}} + \frac{T^*}{t^{(O3)}t_0^{(O3)}}L_G + \frac{t^*}{t^{(O3)}t_0^{(O3)}}L_{WC} + \frac{t^*}{t^{(O3)}t_0^{(O3)}}L_W\right)t^{(O3)}t_0^{(O3)}, \\ L_T^* = \left(L_{path} + TL_G + tL_{WC} + tL_W\right)t^{(O3)}t_0^{(O3)}, \\ L_T = L_{path} + TL_G + tL_{WC} + tL_W. \end{gathered} \tag{2.4}$$

In the above equation, $t_0^{(O3)}$ is the ozone transmittance from the sun to the sea surface, while $t^{(O3)}$ is the ozone transmittance from the sea surface to the sensor. Terms without superscript * indicate that the ozone attenuation effect has been corrected. In the rest of this paper, we will assume that the ozone attenuation effect has been corrected for, unless otherwise noted.

The atmospheric contribution of L_{path} to L_T can be decomposed as follows.

$$L_{path} = L_M + L_A + L_{MA}, \tag{2.5}$$

where L_M is the component due to the scattering of gas molecules only (Rayleigh scattering), L_A is the multiple-scattering component of the aerosol except for the interaction with gas molecules, and L_{MA} represents the interaction between the scattering of gas molecules and aerosol scattering.

Substituting equation (2.5) into equation (2.4) yields the following equation.

$$L_T = L_M + L_A + L_{MA} + TL_G + tL_{WC} + tL_W. \tag{2.6}$$

The purpose of the atmospheric correction is to obtain the water-leaving radiance L_W from the satellite sensor observation radiance L_T based on the model in equation (2.6).

3. Radiative transfer equation for reflectance

3.1 Conversion from radiance-based to reflectance-based

In the atmospheric correction process, the calculation is done on the reflectance basis, not on the radiance basis. The spectral radiance L [Wm^{-2}sr^{-1} μm^{-1}] of the reflected light can be converted to the spectral reflectance ρ as follows.

$$\rho(\lambda, \theta_0) = \frac{\pi L(\lambda)}{F_0(\lambda) \cos\theta_0}, \tag{3.1}$$

where λ is the wavelength, θ_0 is the solar zenith angle, and $\cos\theta_0$ is the incident angle-dependent factor of irradiance and $F_0(\lambda)$ [Wm^{-2} μ m^{-1}] is the extraterrestrial solar irradiance at wavelength λ at the time of observation. It represents the extraterrestrial solar irradiance affected by the daily variation of the Sun-Earth distance. Instantaneous solar irradiance for each SGLI band is calculated from the mean solar irradiance, which is listed in Tables I.1 and I.2 in Appendix I.

The radiance of Eq. (2.6) is converted to reflectance using Eq. (3.1). The terms of radiance L_T, L_M, L_A, L_{MA}, L_G, L_{WC}, and L_W in Eq.(2.6) are converted to the satellite observations Reflectance ρ_T, gas molecule reflectance ρ_M, aerosol reflectance ρ_A, gas molecule and aerosol Reflectivity due to interaction ρ_{MA}, sunglitta reflectivity ρ_G, whitecap reflectivity ρ_{WC} and the water-leaving reflectance ρ_w. It should be noted that the ozone-induced attenuation has already been corrected for, as explained in Chapter 2, and ρ_G, ρ_{WC} and ρ_w are the reflectances observed at the sea surface. The sunlight incident on the sea surface is attenuated by the atmosphere. It is necessary to take into account the transmittance from solar to sea surface t_0 on ρ_G, ρ_{WC} and ρ_w.

Therefore, Eq. (2.6) is transformed as follows,

$$\begin{aligned}
L_T &= L_M + L_A + L_{AM} + TL_G + tL_{WC} + tL_W, \\
\frac{\pi L_T}{F_0 \cos\theta_0} &= \frac{\pi(L_M + L_A + L_{AM})}{F_0 \cos\theta_0} + \frac{\pi(TL_G + tL_{WC} + tL_W)}{F_0 \cos\theta_0 t_0}, \\
\rho_T &= \rho_M + \rho_A + \rho_{AM} + \frac{T\rho_G}{t_0} + \frac{t\rho_{WC}}{t_0} + \frac{t\rho_w}{t_0}, \\
\rho_T &= \rho_M + \rho_A + \rho_{AM} + T[\rho_G]_N + t[\rho_{WC}]_N + t[\rho_w]_N.
\end{aligned} \tag{3.2}$$

where $[\rho_G]_N$ is the normalized water-leaving reflectance $(= \rho_w/t_0)$, $[\rho_{WC}]_N$ is the normalized whitecap reflectance ($= \rho_{wC}/t_0$), and $[\rho_G]_N$ is the normalized sunglint reflectance ($= \rho_G/T_0$). ρ_M, ρ_A, and ρ_{MA} are the atmospheric reflectances at the top of the atmosphere. On the other hand, $[\rho_G]_N$, $[\rho_{WC}]_N$, and $[\rho_w]_N$ refer to the reflectance at sea surface. There are converted to the reflectance of the top of the atmosphere by applying the transmittance T and t from the sea surface to the top of the atmosphere. The satellite-observed reflectance ρ_T is expressed as the sum of these values.

The purpose of the atmospheric correction is to retrieve the water-leaving reflectance $[\rho_w]_N$. $[\rho_G]_N$ is expressed as follows by modifying the Eq. (3.2).

$$\begin{gathered}
\rho_T = \rho_M + \rho_A + \rho_{MA} + T[\rho_G]_N + t[\rho_{WC}]_N + t[\rho_w]_N \ , \\
[\rho_w]_N = \frac{\rho_T - (\rho_M + \rho_A + \rho_{MA} + T[\rho_G]_N + t[\rho_{WC}]_N)}{t} , \\
[\rho_w]_N = \frac{\rho_C - \rho_A - \rho_{MA} - T[\rho_G]_N}{t} - [\rho_{WC}]_N \ ,
\end{gathered} \tag{3.3}$$

where ρ_C is Rayleigh-corrected reflectance which the satellite-observed reflectance ρ_T minus the Rayleigh scattering reflectance ρ_M.

3.2 Relationship between normalized-water leaving radiance and reflectance

Remote sensing reflectance R_{rs}, and normalized water-leaving radiance nL_w are both mostly used physical quantities in ocean color remote sensing. In this section, we describe the relationship between $[\rho_w]_N$ and each of these parameters

The upward spectral radiance at depth z in water is denoted by $L_u(z, \lambda, \theta_0, \theta, \Delta\phi)$, where λ is the wavelength, θ_0 is the solar zenith angle, θ is the satellite zenith angle, and $\Delta\phi$ is the relative azimuth angle between the satellite and the sun. If $\theta = 0$, the sensor faces the nadir, i.e., it observes the radiance of the light toward the zenith. The water-leaving radiance observed just above the sea surface is denoted as $L_w(\lambda, \theta_0, \theta, \Delta\phi)$. L_u is generally obtained from instrumental observations in the water, and L_w is obtained by atmospheric correction of the top of the L_T..

L_u and L_w depend on the irradiance of solar irradiance at the sea surface, E_d. Values independent of E_d is desirable to evaluate the underwater conditions. Therefore, we define the normalized water-leaving radiance nL_w, which excludes the influence of the atmosphere, assuming that the sun is at its zenith.

$$nL_w(\lambda, \theta_0, \theta, \Delta\emptyset) \equiv \frac{L_w(\lambda, \theta_0, \theta, \Delta\emptyset)}{\cos\theta_0\, t(\theta_0)} \quad [W\, m^{-2}\, \mu m^{-1}\, sr^{-1}]$$

where $t(\theta_0)$ is the diffuse transmittance depending on the condition of the atmosphere and the direction of the Sun. In addition, the distance between the Sun and the Earth changes daily and has an inversely proportional effect on the irradiance to the square of the distance. Therefore, $R(T)$ is the distance between the sun and the earth at observation time T, R_0 is the average distance between the sun and the earth. Then $nL_w(\lambda, \theta_0, \theta, \Delta\emptyset)$ is the following in consideration of the correction term $(R/R_0)^2$ (Hereinafter, time of observation T is omitted).

$$nL_w(\lambda, \theta_0, \theta, \Delta\emptyset) \equiv \left(\frac{R}{R_0}\right)^2 \frac{L_w(\lambda, \theta_0, \theta, \Delta\emptyset)}{\cos\theta_0\, t(\theta_0)}, \tag{3.4}$$

That is, nL_w is the water-leaving radiance when the distance between the sun and the earth is equal to its mean value, the sun is at zenith, and there is no atmospheric attenuation of the sunlight.

Next, we consider the conversion from the radiance to the reflectance. According to the definition in Eq. (3.1), the relationship between L_w and the water-leaving reflectance ρ_w is expressed by the following equation,

$$\rho_w(\lambda, \theta_0, \theta, \Delta\emptyset) = \frac{\pi L_w(\lambda, \theta_0, \theta, \Delta\emptyset)}{F_0(\lambda)\cos\theta_0}, \tag{3.5}$$

where $\cos\theta_0$ is an incident angle-dependent factor of irradiance, and F_0 is the extraterrestrial solar irradiance, i.e., the extraterrestrial solar irradiance affected by the daily variation in the Sun-Earth distance. Therefore, F_0 is related with the extraterrestrial solar irradiance $\overline{F_0}$ at the sun-earth mean distance as following,

$$F_0 = \left(\frac{R_0}{R}\right)^2 \overline{F_0} \quad [W\, m^{-2}\, \mu m^{-1}] \cdot \tag{3.6}$$

The relationship between $[\rho_w]_N$ and in-water parameters (ρ_w, L_w, nL_w) is given by Eqs. (3.4), (3.5) and (3. 6), as follow.

$$[\rho_w(\lambda,\theta_0,\theta,\Delta\emptyset)]_N = \frac{\rho_w(\lambda,\theta_0,\theta,\Delta\emptyset)}{t(\theta_0)} = \frac{\pi L_w(\lambda,\theta_0,\theta,\Delta\emptyset)}{F_0(\lambda)\cos\theta_0\, t(\theta_0)}$$
$$= \left(\frac{R}{R_0}\right)^2 \frac{\pi L_w(\lambda,\theta_0,\theta,\Delta\emptyset)}{\overline{F_0(\lambda)}\cos\theta_0\, t(\theta_0)} = \frac{\pi}{\overline{F_0(\lambda)}} nL_w(\lambda,\theta_0,\theta,\Delta\emptyset)\ . \tag{3.7}$$

The remote sensing reflectance R_{rs} is defined by the following equation,

$$R_{rs}(\lambda,\theta_0,\theta,\Delta\emptyset) \equiv \frac{L_w(\lambda,\theta_0,\theta,\Delta\emptyset)}{E_d(0^+,\lambda,\theta_0)} \quad [sr^{-1}]\,. \tag{3.8}$$

In the above equation, 0^+ is the position just above sea surface and $E_d(z,\lambda,\theta_0)$ is the position at altitude z. The reason for the absence of the correction term $(R/R_0)^2$ in Eq. (3.8) is that the mutuality of L_w and E_d to cancel each other out.

The solar irradiance E_d at 0^+ just above the sea surface is the solar irradiance affected by atmospheric attenuation from the top of the atmosphere to the sea surface, and is therefore given by the following equation.

$$E_d(0^+,\lambda,\theta_0) = F_0(\lambda)\cos\theta_0\, t(\theta_0)\ [W\ m^{-2}\ \mu m^{-1}] \tag{3.9}$$

In summary, the following relationship holds between $[\rho_w]_N$, ρ_w, nL_w, L_w and R_{rs}.

$$[\rho_w(\theta_0,\theta,\Delta\emptyset)]_N = \frac{\rho_w(\lambda,\theta_0,\theta,\Delta\emptyset)}{t(\theta_0)} = \frac{\pi}{\overline{F_0}} nL_w(\theta_0,\theta,\Delta\emptyset) = \frac{\pi L_w(\theta_0,\theta,\Delta\emptyset)}{F_0(\lambda)\cos\theta_0\, t(\theta_0)}$$
$$= \frac{\pi L_w(\theta_0,\theta,\Delta\emptyset)}{E_d(0^+,\lambda,\theta_0)} = \pi R_{rs}(\lambda,\theta_0,\theta,\Delta\emptyset) \tag{3.10}$$

Thus, R_{rs} and nL_w are expressed as follows.

$$R_{rs} = \frac{1}{\pi}[\rho_w]_N \quad [sr^{-1}] \tag{3.11}$$

$$nL_w = \frac{F_0}{\pi}[\rho_w]_N \quad [W\ m^{-2}\ \mu m^{-1}\ sr^{-1}] \tag{3.12}$$

The $[\rho_w(\theta_0,\theta,\Delta\emptyset)]_N$ and $R_{rs}(\theta_0,\theta,\Delta\emptyset)$ given in the above equation are thus normalized, or corrected for the effects of the Sun-Earth distance, atmospheric attenuation and solar zenith angle from the observed L_w. However, they still contain a number of direction-dependent parameters such as upward radiance L_u and surface transmittance of water light.

The directional dependency does not simply relies on the direction of the satellite observation but also on the direction of the incident light. Hence it is called Bidirectional Reflectance Distribution Function (BRDF)(Morel and Gentili, 1996). Our atmospheric correction process BRDF correction based on Morel and Gentilli (1996), Morel and Gentilli (2002) and Wang (2006), as described in Chapter 10.

If R_{rs} or nL_w is BRDF-corrected, we use expression such as ${R_{rs}}^{EX}$ or ${nL_w}^{EX}$, respectively, and at the same time, we introduce the BRDF correction factor (C_{BRDF}) as follows.

$$ {R_{rs}}^{EX} = C_{BRDF} \frac{1}{\pi} [\rho_w]_N \quad [sr^{-1}] \text{, and} \tag{3.13} $$

$$ {nL_w}^{EX} = C_{BRDF} \frac{F_0}{\pi} [\rho_w]_N \quad [W\ m^{-2}\ \mu m^{-1}\ sr^{-1}]. \tag{3.14} $$

The calculation of the correction factor (C_{BRDF}) in the above equation will be described in Chapter 10. ${R_{rs}}^{EX}$ and ${nL_w}^{EX}$ are the final outputs of the atmospheric correction.

4. Overview of atmospheric correction for SGLI

The SGLI atmospheric correction method is based on the GLI atmospheric correction method (Toratani et al.,2007) and SeaWiFS atmospheric correction (Gordon and Wang: 1994, Siegel et al.: 2000). A schematic flow of the SGLI atmospheric correction process is shown in Fig. 4.1. The input to the atmospheric correction process is the satellite-observed reflectance ($\rho_T{}^*$), which is converted from the radiance by the Eq. (3.1), The flow of the atmospheric correction process for each pixel is as follows.

(1) Transmittance correction by ozone absorption (Section 7.2)

(2) Correction of the reflectance (ρ_M) of gas molecules (Chapter 5)

(3) High reflectance test

If the Rayleigh-corrected reflectance (ρ_C) of the pixel is greater than 0.07, the atmospheric correction process is skipped.

(4) Sunglitter (ρ_G) correction (Chapter 8)

(5) Whitecap (ρ_{WC}) correction (Chapter 9)

(6) Aerosol reflectance ($\rho_A + \rho_{MA}$) evaluation (Chapter 6)

(7) cloud detection

Aerosol reflectance ($\rho_A + \rho_{MA}$) of 0.04 or more is masked as cloud.

(8) BRDF Correction (Chapter 10)

The normalized water-leaving radiance (nL_w) and remote sensing reflectance (R_{rs}) are calculated through the above process.

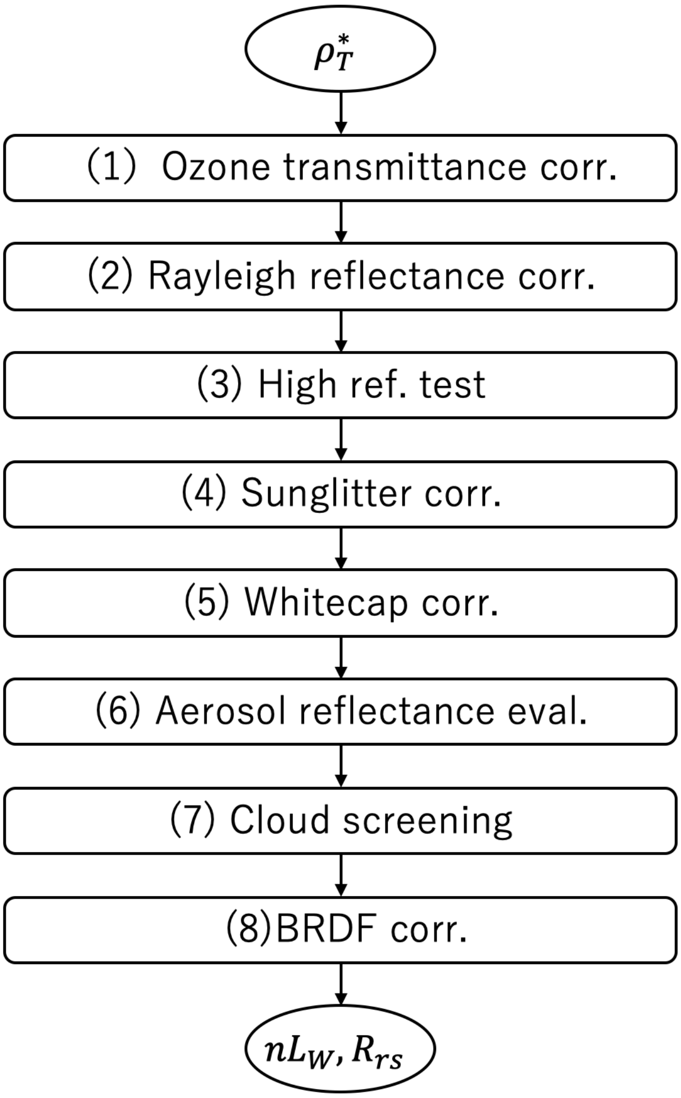

Fig. 4.1 Schematic flow of atmospheric correction for SGLI

5. Rayleigh reflectance (ρ_M)

5.1 Calculation of Rayleigh reflectance

The Rayleigh reflectance ρ_M at wavelength λ is given by the following equation (5.1) based on Gordon et al. (1998), with correction for atmospheric pressure.

$$\rho_M(\lambda) = \frac{1-exp(-\tau_M(\lambda)/cos\theta(\lambda))}{1-exp(-\tau_{M0}(\lambda)/cos\theta(\lambda))}\rho_{M0}(\lambda, \theta(\lambda), \theta_0, \Delta\phi), \quad (5.1)$$

Where

τ_M : Optical thickness of gas molecule,

τ_{M0} : Optical thickness of gas molecule at standard atmospheric pressure, (Table 5.1)

ρ_{M0} : reflectance of gas molecule at standard atmospheric pressure,

$\theta(\lambda)$: Satellite zenith angle for each wavelength (λ),

θ_0 : Solar zenith angle, and

$\Delta\phi$: Relative azimuth angle between sun and satellite.

The reflectance of the gas molecules at standard atmospheric pressure for all the bands are calculated in advance by radiative transfer simulation, and prepared as a lookup table.

The optical thickness of a gas molecule (τ_M) is expressed as follows,

$$\tau_M(\lambda) = \frac{P}{P_0}\tau_{M0}(\lambda) \quad (5.2)$$

where P is the field pressure and P_0 is the standard atmospheric pressure ($=$ $1013.25hPa$).

The optical thickness of the gas molecules at standard atmospheric pressure (τ_{M0}) for all the SGLI bands are shown in Table 5.1. These values were determined by averaging the optical thickness given in the following equation (Bodhaine,1999), weighted by the sensor response function.

$$\tau_{M0}(\lambda) = 0.0021520\left(\frac{1.0455996 - 341.29061\lambda^{-2} - 0.90230850\lambda^2}{1 + 0.0027059889\lambda^{-2} - 85.968563\lambda^2}\right) \quad (5.3)$$

Table 5.1 Rayleigh optical thickness at standard atmospheric pressure in consideration with sensor response function

Band	Rayleigh optical thickness	Band	Rayleigh optical thickness
VN1	0.4467	VN9	0.02571
VN2	0.3189	VN10	0.01525
VN3	0.2361	VN11	0.01525
VN4	0.1559	SW1	0.007107
VN5	0.1132	SW2	0.002380
VN6	0.08714	SW3	0.001246
VN7	0.04265	SW4	0.0003765
VN8	0.04265		

5.2 Look-up table of gas molecular scattering

The reflectance of gas molecules at standard atmospheric pressure is calculated in advance by radiative transfer simulation and stored in a lookup table.

The conditions for creating a lookup table are as follows

θ : 0.0° - 80.5° in increments of 3.5° (24 points)
θ_0 : 0.0° - 80.5° in increments of 3.5° (24 points)
$\Delta\phi$: 0.0° - 180° in 4.0° increments (46 points)
Atmospheric pressure: Standard atmospheric pressure (1013.25 hPa)
Consider polarization
Ignore gas absorption.
Considering multiple scattering
Assuming a plane parallel atmosphere
No sunglint (assuming sea level is flat)
Considering the sensor response function

To calculate the lookup table, we used the radiative transfer simulation code Pstar4 (Ohta et al.,2010).

6. Aerosol reflectance ($\boldsymbol{\rho_A + \rho_{MA}}$)

6.1 Overview of aerosol reflectance calculation

As described in equation (3.2), aerosol-related top-of-atmosphere reflectance are two-fold: ρ_A, the reflectance that would be observed when the atmosphere consists of aerosol particles, and ρ_{MA}, the reflectance due to the interaction between aerosol particles and gas molecules. Hereafter, we refer to the sum of ρ_A and ρ_{MA} as "aerosol reflectance" and use the symbol ρ_{A+MA} to represent it.

The spatio-temporal distribution of aerosol amount and types cannot be predicted in advance. Hence, in the SGLI atmospheric correction, the pixel-wise amount and type of aerosols are determined from the satelite-observed ρ_{A+MA} at the near-infrared and short-wave infrared bands, to estimate ρ_{A+MA} at the visible bands. For this purpose, we define ine aerosol models which have different mixing ratios of tropospheric and oceanic type aerosols (Table 6 .6.1).

The aerosol reflectance determination process is initiated by selecting two models that explain best the aerosol reflectance observed in near-/shortwave-infrared bands. To do so, we use two near-infrared/short-wavelength infrared bands (λ_1 and λ_2). There are two choices for the band pair. The one is λ_1=673 and λ_2=869 nm, while the other pair is λ_1=869 nm and λ_2=1630 nm. The aerosol reflectance correction with the former is called NIR-AC while the correction with the latter is called SWIR-AC. In order to estimate the aerosol reflectance in these bands accurately, the ρ_w in these bands are estimated by using an iterative procedure. In the atmospheric correction, NIR-AC is tried first, and then SWIR-AC is performed when iterations do not converge within the limited number of times, or when the estimated $\rho_w(673)$ is too high (usually caused by high turbidity waters).

6.2 Iterative procedure for aerosol reflectance determination

Schematic flow of iterative aerosol reflectance determination is illustrated in Fig. 6.2.1. The input reflectance is referred to ρ_C, which is the satellite reflectance but with Rayleigh, sunglint, and whitecap corrections applied beforehand. Hence, ρ_C is understood as the sum of the aerosol reflectance (ρ_{A+MA}) and the normalized water-leaving reflectance multiplied by the transmittance (t$[\rho_w]_N$).

$$\rho_C(\lambda) = \rho_{A+MA}(\lambda) + t(\lambda)[\rho_w]_N(\lambda) \tag{6.2.1}$$

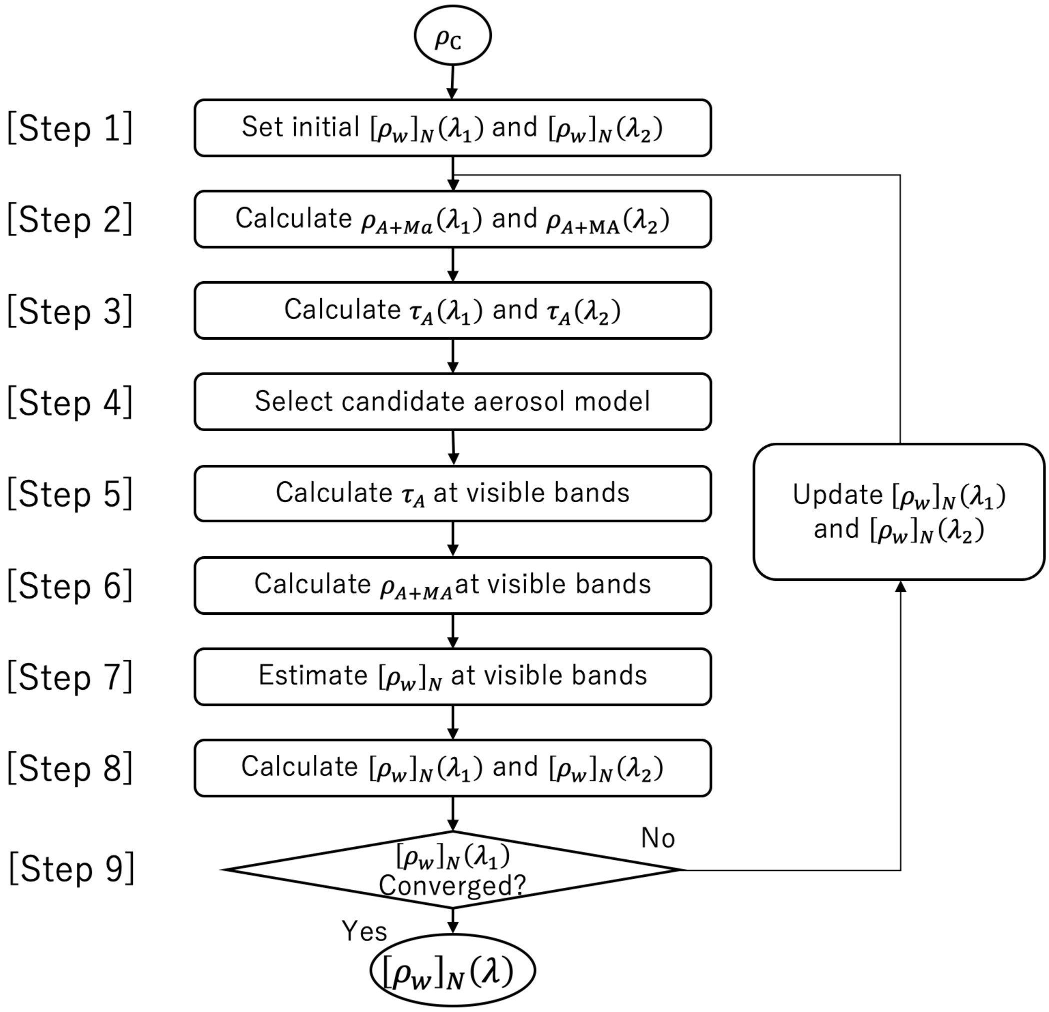

Fig.6.2.1 Schematic flow of aerosol reflectance

The iterative procedure for aerosol reflectance determination is carried out as follows.

[Step 1] Set initial value of $[\rho_w]_N$ in the near-infrared region

The initial value of $[\rho_w]_N(869)$ is set to zero. The initial value of $[\rho_w]_N(673)$ is entered as the maximum possible value when the condition that results in the lowest $\rho_{A+MA}(673)$ assumes the oceanic aerosol (model 9) and $t(673)$ and $t_0(673)$ for 1.0.

[Step2] Calculation of $\boldsymbol{\rho_{A+MA}}$ in the near-infrared

With the preset (or later updated) values of $[\rho_w]_N$ in the NIR/SWIR bands, $\rho_{A+MA}(673)$ and $\rho_{A+MA}(869)$ are determined for NIR-AC. $\rho_{A+MA}(1630)$ is also deteremined for SWIR-AC. In what follows, (λ_1, λ_2) is (673, 869) for NIR-AC, or (869, 1630) for SWIR-AC.

[Step 3] Conversion of $\boldsymbol{\rho_{A+MA}}$ to $\boldsymbol{\tau_A}$ in the near-infrared and short-wavelength infrared region

To select an aerosol model, $\rho_{A+MA}(\lambda_1)$ and $\rho_{A+MA}(\lambda_2)$ is converted to $\tau_A(\lambda_1)$ and $\tau_A(\lambda_2)$. The conversion is made through reference to the aerosol LUT (section 6.5), which contains the relationship between reflectance and optical thickness for each of the nine "aerosol models". Hence, assuming each model, we obtain nine pairs of model-dependent estimates, $\tau_A(M, \lambda_1)$ and $\tau_A(M, \lambda_2)$.

[Step 4] Selection of the two aerosol models

The wavelength-to-wavelength ratio of the aerosol optical thickness (γ) is dependent on different aerosol types. Therefore, the ratio $(\gamma(\lambda_1, \lambda_2))$, shown below, is used to select the two aerosol models out of the nine standard models.

$$\gamma(\lambda_1, \lambda_2) = \frac{\tau_A(\lambda_1)}{\tau_A(\lambda_2)} \tag{6.2.2}$$

In order to estimate the aerosol optical thickness, the relationship between reflectance and optical thickness, which is contained in the aerosol LUT, is used. However, this "relationship" is different for each model aerosol (M). Therefore, the ratio of aerosol optical thicknesses estimated from satellites, γ_E, is defined for each model.

$$\gamma_E(M, \lambda_1, \lambda_2) = \frac{\tau_A(M, \lambda_1)}{\tau_A(M, \lambda_2)} \tag{6.2.3}$$

On the other hand, the theoretical value for the ratio of the optical thickness of the aerosol for each aerosol model (γ_T) is generally different from that of γ_E. Since the ratio of optical thickness γ_T is equal to the ratio of the extinction coefficient of the aerosol (k_{ext}), γ_T is expressed as follows.

$$\gamma_T(M,\lambda_1,\lambda_2) = \frac{k_{ext}(M,\lambda_1)}{k_{ext}(M,\lambda_2)} \tag{6.2.4}$$

In the actual implementation of the atmospheric corrections, relative value of k_{ext} for each wavelength, normalized by $k_{ext}(869)$, is stored in a table (Appendix II).

Aerosol model selection uses γ_{AVE}, the average of $\gamma_E(M,\lambda_1,\lambda_2)$. After a refining process of averaging, the final γ_{AVE} is used to determine two aerosol models M_1 and M_2 that have closest γ_T values to γ_{AVE}. Detailed description of the refining process can be found in Fukushima et a. (1998).

The interpolation ratio r between the two selected models M_1 and M_2, is defined as follows.

$$r = \frac{\gamma_{AVE} - \gamma_T(M_1,\lambda_1,\lambda_2)}{\gamma_T(M_2,\lambda_1,\lambda_2) - \gamma_T(M_1,\lambda_1,\lambda_2)} \tag{6.2.5}$$

[Step 5] Estimation of τ_A in the visible region by two selected aerosol models.

For each of the candidate model M_1 and M_2, the τ_A values at the visible bands are calculated by the following relation.

$$\tau_A(M,\lambda) = \frac{k_{ext}(M,\lambda)}{k_{ext}(M,\lambda_2)}\tau_A(M,\lambda_2)\,, \tag{6.2.6}$$

where M is either of the two selected models M_1 and M_2, whereas λ denotes visible band, which is either of 380, 412, 443, 490, 530, and 565 nm for NIR-AC case. For SWIR-AC, the "visible" band set includes 673 nm.

[Step 6] Conversion from τ _A to ρ _(A+MA) in the visible region.

From the $\tau_A(M,\lambda)$ for each wavelength in the visible region, the lookup table (see Section 6.5) is used to calculate the visible region to $\rho_{A+MA}(M,\lambda)$ in the region, where M is one of the two selected models M_1 and M_2.
Using ρ_{A+MA} for selected M_1 and M_2 and the interpolation ratio *r*, we get ρ_{A+MA} for each visible band as follows.

$$\rho_{A+MA}(\lambda) = (1-r)\rho_{A+\mathrm{MA}}(M_1,\lambda) + r\rho_{A+MA}(M_2,\lambda) \tag{6.2.7}$$

We also determine τ_A for each wavelength in the same way.

$$\tau_A(\lambda) = (1-r)\tau_A(M_1,\lambda) + r \cdot \tau_A(M_1,\lambda) \tag{6.2.8}$$

This $\tau_A(\lambda)$ is used for the calculation of the aerosol transmittance in the following iterative process.

[Step 7] Estimation of $[\rho_w]_N$ in the visible region

From the obtained ρ_{A+MA} in the visible region, $[\rho_w]_N$ in the visible region is estimated as follows,

$$[\rho_w]_N(\lambda) = \frac{\langle \rho_C(\lambda) - \rho_{A+MA}(\lambda) \rangle}{t(\lambda)} \tag{6.2.9}$$

[Step 8] Estimation of $[\rho_w]_N$ in the near-infrared region

From $[\rho_w]_N(\lambda)$ in the visible region, $[\rho_w]_N(673)$ and $[\rho_w]_N(869)$ is calculated, or updated, through the in-water model (see Section 6.3) in the case of NIR-AC. For SWIR-AC, only the value $[\rho_w]_N(869)$ is required to be updated.

[Step 9] Check for convergence

The convergence of the iteration (step 2 through 9) is checked as follows. Let $[\rho_w]_N(\lambda_1)_n$ be the n-th updated $[\rho_w]_N(\lambda_1)$ value in step 8, where n is the number of iteration, n=0, 1, 2, ⋯ . Note that $[\rho_w]_N(\lambda_1)_0$ means the initial value defined in Step 1. Then, if the following condition,

$$|[\rho_w]_N(\lambda_1)_{n+1} - [\rho_w]_N(\lambda_1)_n| < Threshold \ , \tag{6.2.10}$$

does not holds, and if n is less than 10, the new iteration from Step 2 through Step 8 is conducted. Otherwise, the iteration is terminated.

The condition of convergence (Threshold) was set to 0.00001 for both NIR-AC and SWIR-AC.

6.3 Estimation of water-leaving reflectance at near infrared bands

The normalized water-leaving reflectance in the near-infrared does not vary independently of the visible water-leaving reflectance, but varies in conjunction with water conditions such as chlorophyll a concentration and suspended matter concentration.

An overview of the $[\rho_w]_N$ estimation in the near-infrared region is shown in Fig. 6.3.1. The estimation of $[\rho_w]_N(673)$ is based on the Quasi Analytical Algorithm (QAA) (Lee et al, 2002), where estimation of inherent optical properties (IOPs) is done by an empirical formula to simplify the calculation. The estimation of $[\rho_w]_N(869)$ is also done empirically through an in-water model based on Ahn et al. (2015).

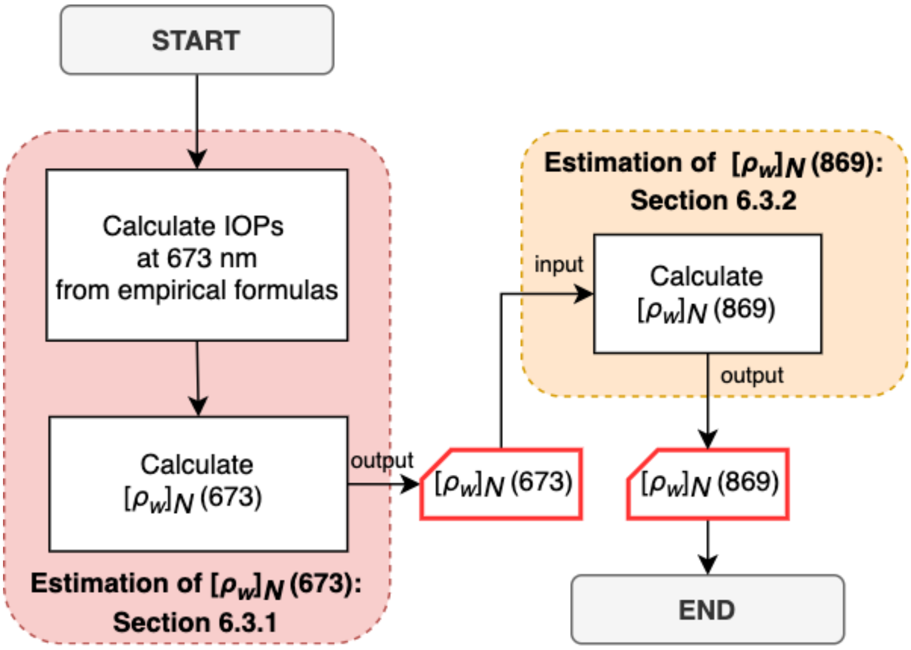

Figure 6.3.1 Schematic flow of algorithm estimating $[\rho_w]_N$ in Red-NIR

6.3.1 Estimation of $[\rho_w]_N(673)$

The $[\rho_w]_N$ at wavelength λ can be expressed by the following relationship for IOPs (Lee et al, 2002).

$$[\rho_w]_N(\lambda) = \pi R_{rs}(\lambda) = \pi \frac{0.52 r_{rs}(\lambda)}{1 - 1.7 r_{rs}(\lambda)}, \tag{6.3.1}$$

$$r_{rs}(\lambda) = [0.089 + 1.125 u(\lambda)] u(\lambda), \tag{6.3.2}$$

$$u(\lambda) = \frac{b_b(\lambda)}{a(\lambda) + b_b(\lambda)}, \tag{6.3.3}$$

$$a(\lambda) = a_w(\lambda) + a_{exw}(\lambda), \text{ and} \tag{6.3.4}$$

$$b_b(\lambda) = b_{bw}(\lambda) + b_{bp}(\lambda) \ , \tag{6.3.5}$$

where r_{rs} is the remote sensing reflectance just below the ocean surface, a and b_b are the total absorption and backscattering coefficients of water, a_w and b_{bw} are the absorption and backscattering coefficients of pure seawater, a_{exw} is the sum of the absorption coefficients for all the constituents other than water (phytoplankton, CDOM, etc.), and b_{bp} is the backscattering coefficient due to suspended particles.

The $[\rho_w]_N(673)$ is estimated from the above equations, where $a(673)$ and $b_b(673)$ in Eq. (6.3.3) are estimated using empirical formulae.

The estimation procedure is shown in Fig. 6.3.2.

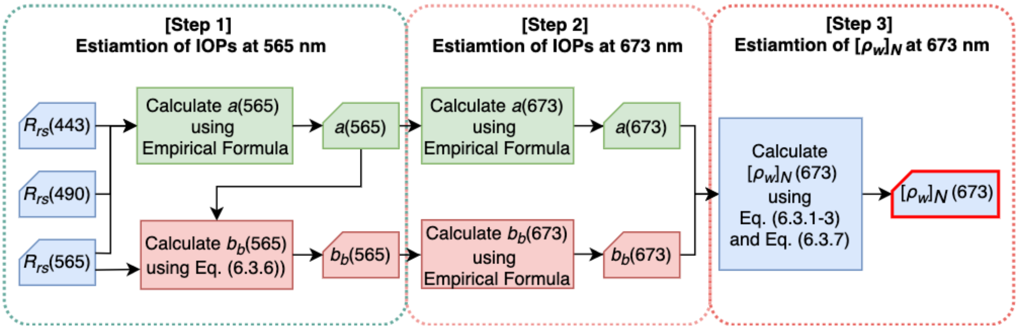

Figure 6.3.2 Estimation flow of $[\rho_w]_N(673)$

[STEP 1] Estimation of IOPs at 565 nm:

Estimation of $a(565)$ is done empirically form $R_{rs}(443)$, $R_{rs}(490)$ and $R_{rs}(565)$ (Ahn, personal comm.). The details are omitted.

$b_b(565)$ is obtained from $R_{rs}(565)$ and $a(565)$ from Eq. (6.3.6), where b_b is from the equation (Z. P. Lee et al., 2002).

$$b_b(565) = \frac{a(565)\,u(565)}{1 - u(565)},$$
$$u(565) = \frac{-0.0895 + \sqrt{0.00801 + 0.499 r_{rs}(565)}}{0.249}, \quad (6.3.6)$$
$$r_{rs}(565) = \frac{R_{rs}(565)}{0.52 + 1.7 R_{rs}(565)}.$$

[STEP 2] Estimation of IOPs at 673 nm:

The values for $a(673)$ and $b_b(673)$ are estimated from $a(565)$ and $b_b(565)$ through an empirical formula (Ahn, personal comm.). Details are omitted.

[STEP 3] The estimation of $[\rho_w]_N$ at 673 nm:

$[\rho_w]_N(673)$ is determined by equations (6.3.1)- (6.3.3) with $a(673)$ and $b_b(673)$ values obtained in STEP 2.

The results of validation of the model with the MOBY and AERONET-OC measurements are shown in Fig. 6.3.3. The validation was performed after converting the model to nLw.

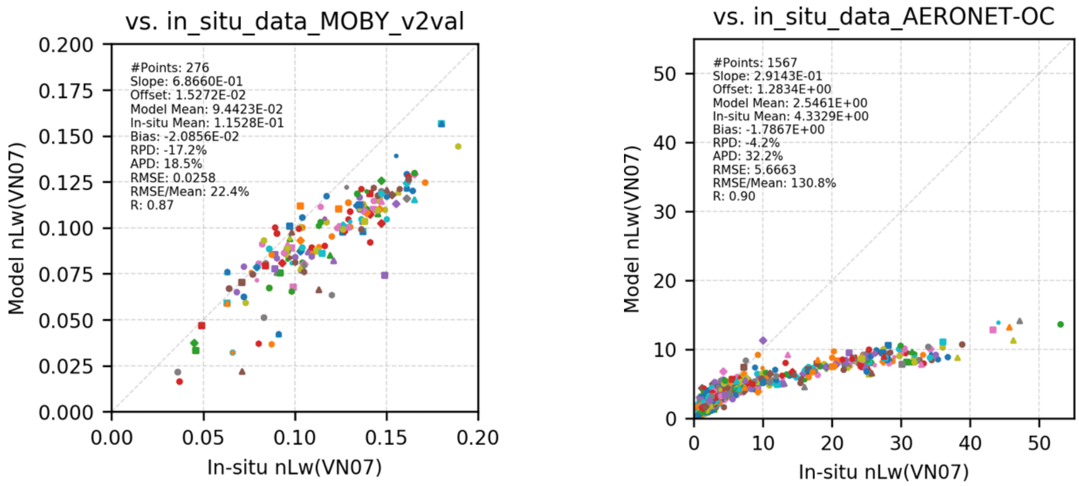

Figure 6.3.3 Comparison between *In-situ* and predicted values

As is shown in the figure, when *in-situ* $nL_W(673)$ is higher than 7 W m^{-2} sr^{-1} μm^{-1}, it tends to be underestimate. The reason for this is that the effects of inorganic suspended matter such as soil particles in coastal areas are not fully considered. To deal with this problem, the following correction equation was derived based on the comparison between *in-situ* and estimated data (Fig,6.3.4).

$$[\rho_w]_N(673) = C[\rho_w]_N^*(673),$$
$$C = \begin{cases} 3.7 & (c > 3.7) \\ c & (c \leq 3.7) \end{cases}, \qquad (6.3.7)$$
$$c = 2.3122 \times 10^4 x^2 - 5.7814 \times 10x + 1.2365,$$
$$x = [\rho_w]_N^*(673),$$

where $[\rho_w]_N^*(673)$ represents original estimate of $[\rho_w]_N(673)$.

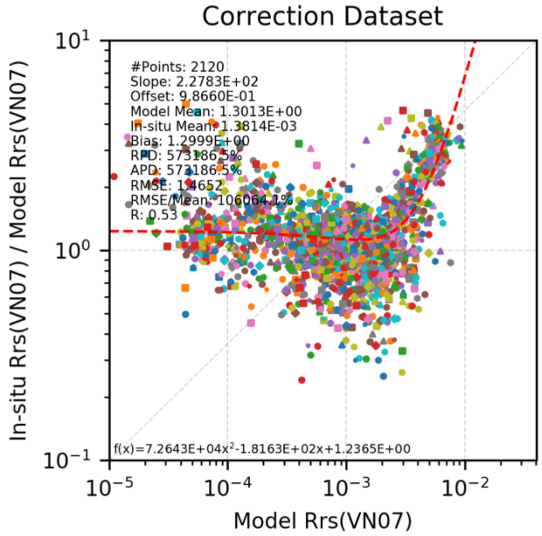

Figure 6.3.4 Ratio of *In-situ* to predicted values

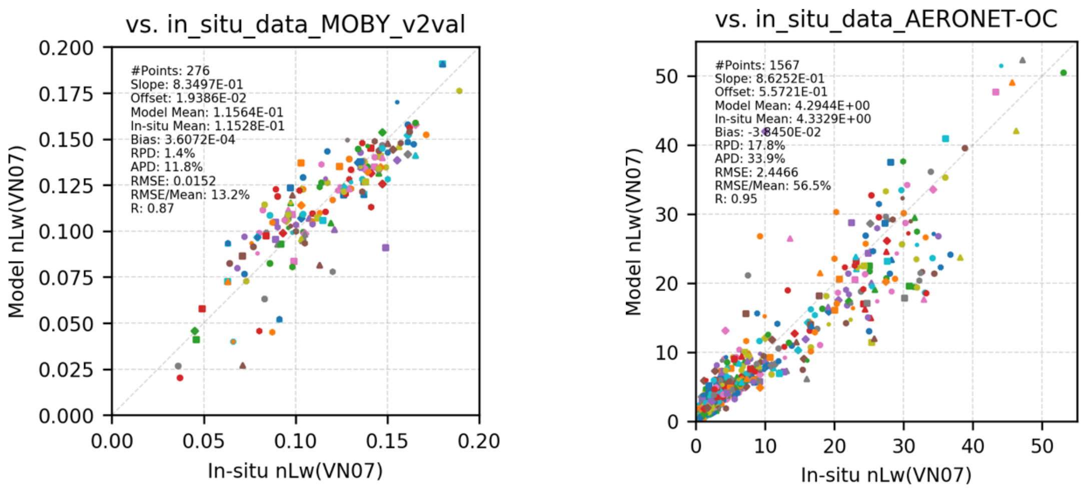

Figure 6.3.5 Comparison between *In-situ* and corrected values

Table 6.3.1 Accuracies of $nL_w(673)$

) MOBY	RMSE*	RMSE/Mean	Bias*	R
Uncorrected	0.0258	22.4%	-2.09E-2	0.87
Corrected	0.0152	13.2%	3.61E-4	0.87

) AERONET-OC	RMSE	RMSE/Mean	Bias	R
Uncorrected	5.6663	130.8%	-1.79E0	0.90
Corrected	2.4466	56.5%	-3.85E-2	0.95

* Unit: W m^{-2} sr^{-1} μm^{-1}

Fig. 6.3.5 shows the validation results for the estimated values with correction. The accuracy before and after the correction is shown in Table 6.3.1, which shows improvement by 40-60% in terms of RMSE. We apply this correction of Eq. (6.3.7) to $[\rho_w]_N(673)$.

6.3.2 Estimation of $[\boldsymbol{\rho_w}]_N(\mathbf{869})$

$[\rho_w]_N(869)$ is estimated by the following equation, which was derived from Eqs. (24) and Eq. (25) in Ahn et al. (2015)

$$[\rho_w]_N(869) = 2269.3x^4 - 326.32x^2 + 16.147x - 0.1592, \quad x = [\rho_w]_N(673) \quad (6.3.8)$$

where $[\rho_w]_N(673)$ is the result from Eq. (6.3.7).

6.4 Switching between NIR-AC and SWIR-AC

The combination of wavelengths in the aerosol model selection, for normal atmospheric correction (NIR-AC), is 673 nm and 869 nm, as in the case of high-suspended matter concentrations, the combination switch to 869 nm and Switch to 1630 nm (SWIR-AC).

The conditions for the switch are as follows,

Condition 1 $nL_W(673) > 10[W \cdot sr^{-1} \cdot m^{-2} \cdot \mu m^{-1}]$

Condition 2 When the iterative operations do not converge

Condition 3 $nL_W(490) < 0$

The only difference between NIR-AC and SWIR-AC is the combination of wavelengths. The calculation procedure is the same. The wavelength of $[\rho_w]_N$, which is used as the convergence condition is changed from 673 to 869nm in SWIR-AC.

6.5 Lookup tables of aerosol

There are two aerosol lookup tables used to calculate aerosol reflectance. The first is a table that converts ρ_{A+MA} to τ_A, while the other is a table that converts τ_A to ρ_{A+MA}. The former is used in the selection of aerosol models in the near-infrared and short-wavelength infrared bands. The latter is used to determine the aerosol reflectance in the visible region for the assumed aerosol model.

The first lookup table stores the following quadratic equation coefficients (a_0, a_1, a_2, a_3, and a_4) for conversion from ρ_{A+MA} to τ_A. Note that a_0 is always zero.

$$\tau_A(M, \lambda, \theta, \theta_0, \Delta\phi) = a_0 + a_1 X + a_2 X^2 + a_3 X^3 + a_4 X^4 \ , \tag{6.5.1}$$

where

$X = \rho_A(M, \lambda, \theta, \theta_0, \Delta\phi) + \rho_{MA}(M, \lambda, \theta, \theta_0, \Delta\phi)$,

M : Aerosol Models,

θ : Satellite zenith angle,

θ_0 : Solar zenith angle,

$\Delta\phi$: Relative azimuth angle of the sun and the satellite.

The second look-up table that convert τ_A to ρ_{A+MA} similarly stores the coefficients a_0, a_1, a_2, a_3, and a_4 of the following quadratic equation, where a_0 is assumed to be zero.

$$\rho_{A+MA}(M, \lambda, \theta, \theta_0, \Delta\phi) = a_0 + a_1 Y + a_2 Y^2 + a_3 Y^3 + a_4 Y^4 \ , \tag{6.5.2}$$

where

$Y = \tau_A(M, \lambda, \theta, \theta_0, \Delta\phi)$.

Aerosol lookup tables were prepared in advance by the radiative transfer simulation code Pstar4 (Ohta et al.,2010). The conditions for the calculations were as follows.

θ : 0.0° - 80.5° in increments of 3.5° (24 points)

θ_0 : 0.0° - 80.5° in increments of 3.5° (24 points)

$\Delta\phi$: 0.0° - 180° in 4.0° increments (46 points)

Considering polarization

Considering multiple scattering

Assuming a plane parallel atmosphere

No sunglint (assuming sea level is flat)

Considering the sensor response function

Model-wise “optimized” maximum aerosol optical thickness settings (Table 6.5.2)

To calculate the aerosol reflectance for each aerosol model under the pixel-wise scan geometry θ, θ_0, and $\Delta\phi$, we use three dimensional interpolation to determine the a_n values for the pixel. The interpolation is based on a linear Lagrange interpolation for $\theta \leq 60°$ and $\theta_0 \leq 60°$, whereas if $\theta > 60°$ or $\theta_0 >$

60°, second-order Lagrange interpolation is used.

(1) Coefficient for $\theta \leq 60°$ and $\theta_0 \leq 60°$.

The coefficients in equations (6.5.1) and (6.5.2) when $\theta \leq 60°$ and $\theta_0 \leq 60°$ are calculated as follows.

$$a_n(\theta, \theta_0, \Delta\phi) = \sum_{i=u}^{u+1} \sum_{j=v}^{v+1} \sum_{k=w}^{w+1} A_{n,ijk} L_i(\theta) M_j(\theta_0)\, N_k(\Delta\phi) \tag{6.5.3}$$

The grid index triplet (*u, v, w*) is chosen so that it meets the following .

$$\theta_u < \theta < \theta_{u+1}$$
$$\theta_{0\,v} < \theta_0 < \theta_{0\,v+1}$$
$$\Delta\phi_w < \Delta\phi < \Delta\phi_{w+1}$$

where

$0 \leq u \leq 22,\ 0 \leq v \leq 22,\ 0 \leq w \leq 44,$
$A_{n,ijk}$: Coefficients stored in the lookup table of grid numbers i, j and k
Since the number of divisions of θ is 24, i=0,.... ,23
Since the number of divisions of θ _0 is 24, j=0,.... ,23
The number of divisions of Δ φ is 46, k=0,.... ,45

The interpolation coefficients $L_u(\theta)$ and $L_{u+1}(\theta)$ are defined as

$$L_u(\theta) = \frac{\theta - \theta_{u+1}}{\theta_u - \theta_{u+1}}\ \text{, and}$$
$$L_{u+1}(\theta) = \frac{\theta - \theta_u}{\theta_{u+1} - \theta_u}\,. \tag{6.5.4}$$

The interpolation coefficients $M_j(\theta_0)$ and $N_k(\Delta\phi)$ are defined in similar way.

(2) Coefficient for $\theta > 60°$ or $\theta_0 > 60°$

The coefficients in equations (6.5.1) and (6.5.2) when $\theta > 60°$ or $\theta_0 > 60°$ are calculated as follows.

$$a_n(\theta, \theta_0, \Delta\phi) = \sum_{i=u}^{u+2} \sum_{j=v}^{v+2} \sum_{k=w}^{w+2} A_{n,ijk} L_i(\theta) M_j(\theta_0)\, N_k(\Delta\phi) \tag{6.5.5}$$

The grid index triplet (u, v, w) is determined so that θ, θ_0 and $\Delta\phi$ for the grid ($u+1$, $v+1$ and $w+1$) has the closest values to those of the pixel. Then, the interpolation coefficient L is given by:

$$L_u(\theta) = \frac{(\theta - \theta_{u+1})(\theta - \theta_{u+2})}{(\theta_u - \theta_{u+1})(\theta_u - \theta_{u+2})},$$
$$L_{u+1}(\theta) = \frac{(\theta - \theta_u)(\theta - \theta_{u+2})}{(\theta_{u+1} - \theta_u)(\theta_{u+1} - \theta_{u+2})}, \text{and} \tag{6.5.6}$$
$$L_{u+2}(\theta) = \frac{(\theta - \theta_u)(\theta - \theta_{u+1})}{(\theta_{u+2} - \theta_u)(\theta_{u+2} - \theta_{u+1})},$$

where 0≤u≤21, 0≤v≤21 and 0≤w≤43. The values of $M_j(\theta_0)$ and $N_k(\Delta\phi)$ are similarly defined.

Table 6.5.1 Aerosol models

	Aerosol volume ration		Relative Humidity (%)
	Tropospheric	Oceanic	
Model1	1	0	70
Model2	1	0.32	70
Model3	1	0.64	70
Model4	1	1.28	70
Model5	1	2.56	60
Model6	1	2.56	73
Model7	1	5.14	70
Model8	1	10.39	70
Model9	0	1	83

The tropospheric and oceanic model is described in Shettle and Fenn (1979).

Table 6.5.2 Upper limit of aerosol optical thickness for each band and aerosol model

Band (nm)	M1	M2	M3	M4	M5	M6	M7	M8	M9
380	1.7	1.5	1.4	1.2	1.1	1.1	0.9	0.8	0.8
412	1.6	1.4	1.3	1.2	1.0	1.0	0.9	0.8	0.8
443	1.5	1.3	1.2	1.1	0.95	0.95	0.9	0.8	0.8
490	1.3	1.2	1.1	1.0	0.9	0.9	0.85	0.8	0.8
530	1.2	1.1	1.0	1.0	0.85	0.87	0.8	0.8	0.8
565	1.1	1.0	0.93	0.9	0.8	0.85	0.8	0.8	0.8
670	0.9	0.8	0.8	0.8	0.72	0.76	0.75	0.75	0.85
763	0.7	0.7	0.7	0.7	0.7	0.7	0.7	0.7	0.85
865	0.6	0.6	0.6	0.6	0.6	0.7	0.7	0.7	0.85
1050	0.4	0.5	0.5	0.5	0.52	0.6	0.6	0.7	0.85
1380	0.3	0.4	0.4	0.4	0.45	0.55	0.55	0.6	0.83
1630	0.15	0.3	0.3	0.35	0.4	0.5	0.5	0.6	0.81
2210	0.05	0.2	0.2	0.25	0.3	0.4	0.4	0.5	0.75

7. Transmittance

The atmospheric correction process takes into account the transmittance, such as attenuation due to scattering of gas molecules and absorption by gas molecules of ozone, nitrogen dioxide, and oxygen. When we refer to the transmittance, there are two pathways to consider. One is from the top of atmosphere (the sun) to the sea surface, whereas the other is from the sea surface to the satellite. Transmittance *t* for the former is written as t_0 with subscript 0 while the one for the latter is described without the subscript.

7.1 Molecule transmittance

The diffuse transmittance of gas molecules is evaluated as half the optical thickness of gas molecules contributes to the extinction, since the amount of forward and back scattering is the same.

$$
\begin{aligned}
t^{(M)}(\lambda) &= exp\left(-\frac{\tau_M(\lambda)}{2\cdot cos\,\theta}\right) \;, \\
t_0^{(M)}(\lambda) &= exp\left(-\frac{\tau_M(\lambda)}{2\cdot cos\,\theta_0}\right) \;,
\end{aligned}
\tag{7.1}
$$

where $\tau_M(\lambda)$ is the optical thickness of the gas molecule shown in Eq. (5.2).

The direct transmittance of gas molecule is expressed by the following equation, since any scattering is considered to contribute to the attenuation.

$$
\begin{aligned}
T^{(M)}(\lambda) &= exp\left(-\frac{\tau_M(\lambda)}{cos\,\theta}\right) \\
T_0^{(M)}(\lambda) &= exp\left(-\frac{\tau_M(\lambda)}{cos\,\theta_0}\right)
\end{aligned}
\tag{7.2}
$$

7.2 Ozone transmittance

The transmittance of ozone is expressed by the following equation.

$$
\begin{aligned}
t^{(O3)}(\lambda) &= exp\left(-\frac{\tau_{OZ}(\lambda)}{cos\,\theta}\right), \text{and} \\
t_0^{(O3)}(\lambda) &= exp\left(-\frac{\tau_{OZ}(\lambda)}{cos\,\theta_0}\right).
\end{aligned}
\tag{7.3}
$$

The ozone optical thickness $\tau_{OZ}(\lambda)$ is expressed as

$$\tau_{OZ}(\lambda) = DU \cdot k_{OZ}(\lambda) \ , \tag{7.4}$$

where Dobson Unit (DU, Section 11.1) is the virtual thickness of the columnar ozone, under assumed standard condition (1 atm, 0° C), while $k_{OZ}(\lambda)$ is the extinction coefficient of ozone at wavelength λ per DU. The values of $k_{OZ}(\lambda)$ are shown in Table 7.1. It was calculated from the ozone absorption cross-section data (Voigt et al., 2001) in consideration with the sensor response function.

Table 7.1 Extinction coefficient of ozone for SGLI bands, weighted by the sensor response function.

Band	$<k_{OZ}(\lambda)>$[DU^{-1}]	Band	$<k_{OZ}(\lambda)>$[DU^{-1}]
VN1	7.97e-08	VN9	7.59e-06
VN2	4.33e-07	VN10	2.10e-08
VN3	3.74e-06	VN11	2.10e-08
VN4	2.25e-05	SW1	0.00e+00
VN5	6.79e-05	SW2	0.00e+00
VN6	1.17e-04	SW3	0.00e+00
VN7	4.42e-05	SW4	0.00e+00
VN8	4.42e-05		

7.3 aerosol transmittance

The diffuse transmittance of the aerosol is calculated using the following formula.

$$t^{(A)}(\lambda) = exp\left\{-\frac{(1-\omega_A(\lambda)\eta)\tau_A(\lambda)}{cos\ \theta}\right\}, \text{and}$$
$$t_0^{(A)}(\lambda) = exp\left\{-\frac{(1-\omega_A(\lambda)\eta)\tau_A(\lambda)}{cos\ \theta_0}\right\}, \tag{7.5}$$

where ω_A is the single-scattering albedo of the aerosol and η is the forward scattering probability (η = 1). The single-scattering albedo for each aerosol model is described in Appendix III. The aerosol optical thickness $\tau_A(\lambda)$ for the target pixel is calculated by Eq.(6.2.8).

The direct transmittance of aerosol is expressed as follows.

$$T^{(A)}(\lambda) = exp\left\{-\frac{\tau_A(\lambda)}{cos\ \theta}\right\}\text{, and}$$
$$T_0^{(A)}(\lambda) = exp\left\{-\frac{\tau_A(\lambda)}{cos\ \theta_0}\right\}. \qquad (7.6)$$

8. Sunglitter correction

The reflectance of the sunglitter, which is defined just above the sea surface, is given as follows (Cox and Munk: 1954a, 1954b and 1956).

$$\rho_g(\lambda) = T_0(\lambda)\frac{\pi f(\omega,\lambda)P_W(\theta,\theta_0,\Delta\phi,W)}{4\cdot cos\theta\cdot cos\theta_0\cdot cos^4\theta_n}, \tag{8.1}$$

whereas the normalized sunglitter reflectance $[\rho_G]_N$, defined against the extraterrestrial solar irradiance, is given by

$$\left[\rho_g(\lambda)\right]_N = \frac{\pi f(\omega,\lambda)P_W(\theta,\theta_0,\Delta\phi,W)}{4\cdot cos\theta\cdot cos\theta_0\cdot cos^4\theta_n}, \tag{8.2}$$

since $\left[\rho_g(\lambda)\right]_N = {\rho_g(\lambda)}/{T_0}$, as defined in Eq. (3.2).

In the above equations, T_0 is the beam transmittance for the downward solar light, $P_W(\theta,\theta_0,\Delta\phi,W)$ is the probability of the facet of the sea surface generates the sunglitter. The latter is further shown as follows.

$$P_W(\theta,\theta_0,\Delta\phi,W) = \frac{1}{\boldsymbol{\pi}\sigma^2}exp\left(\frac{-tan^2\theta_n}{\sigma^2}\right). \tag{8.3}$$

The term σ^2 is expressed as a function of the wind speed (W) and is given by the following equation.

$$\sigma^2 = 0.003 + 0.00512W$$

The θ_n term is the zenith angle of a normal $\boldsymbol{n}$ to the sea surface facet from which the sunglitter arises, and is shown as follows.

$$\theta_n = cos^{-1}\left(\frac{cos\theta + cos\theta_0}{2cos\omega}\right),$$

where ω is the angle between the directions of the $\boldsymbol{n}$ and the sun or the satellite, expressed as

$$cos2\omega = cos\theta cos\theta_0 + sin\theta sin\theta_0 cos\Delta\phi$$

$f(\omega,\lambda)$) is the Fresnel reflectance as follows,

$$f(\omega,\lambda) = 1 - (2\cdot n(\lambda)\cdot y\cdot z)\,cos\omega\,,$$

$$y = \frac{\sqrt{n(\lambda)^2 + cos^2\omega - 1}}{n(\lambda)}\text{, and}$$

$$z = \frac{1}{\{cos\omega + yn(\lambda)\}^2} + \frac{1}{\{y + n(\lambda)cos\omega\}^2},$$

where $n(\lambda)$ is the refractive index.

Since the contribution of sunglitter reflectance to the satellite-observed reflectance ρ_T is $T[\rho_G]_N$ as shown below,

$$\rho_T = \rho_M + \rho_A + \rho_{AM} + T[\rho_G]_N + t[\rho_{WC}]_N + t[\rho_w]_N, \tag{3.2}$$

we further need to determine the beam transmittance $T(\lambda)$ between the sea-surface and the satellite. As far as the sunglitter correction is concerned, we assume constant optical thickness $\tau_A(869)$ of 0.1, which seems to be appropriate based on the global SeaWiFS observation over the ocean (Wang, 2001). The τ_A values for other wavelengths are also set to 0.1, meaning that we anticipate the oceanic type aerosol (see models 8 and 9 in Appendix II).

9. Whitecap correction

The equation for the reflectance $[\rho_{WC}]_N$ due to the whitecap of the sea surface is expressed as follows.

$$[\rho_{WC}]_N(\lambda) = k_{WC}(\lambda) \cdot R_{WC} \cdot W_{dc}\,, \tag{9.1}$$

where

$k_{WC}(\lambda)$: wavelength dependence coefficient (Table 9.1; Frouin et al., 1996)

R_{WC} : Koepke's effective reflectance in white caps (=0.22)

W_{dc}: Wind speed dependency coefficient (Stramska and Petelski,2003)

$$W = 8.75 \times 10^{-5}(U_{10} - 6.33)^3$$

U_{10} is the wind speed at an elevation of 10 m.

The minimum wind speed is assumed to be 6.33ms^{-1}. If U_{10} is below the minimum, $[\rho_{WC}]_N(\lambda) = 0$.

Table 9.1 Wavelength dependent factor

Band	$\boldsymbol{k_{WC}(\lambda)}$	Band	$\boldsymbol{k_{WC}(\lambda)}$
VN1	1.0	VN9	0.762766
VN2	1.0	VN10	0.640922
VN3	1.0	VN11	0.640922
VN4	1.0	SW1	0.526908
VN5	1.0	SW2	0.319608
VN6	0,990367	SW3	0.156282
VN7	0.884466	SW4	0.0
VN8	0.884466		

10. Bidirectional reflectance distribution function (BRDF)

$nL_w(\lambda, \theta, \theta_0, \Delta\phi)$ and $R_{rs}(\theta_0, \theta, \Delta\emptyset)$ are "normalized" quantities, in the sense that those are derived from the observed L_w with corrections of the effects arising from variability of the Sun-Earth distance, atmospheric transmittance and solar zenith angle. However, they still contain direction-dependent factors of upward radiance L_u and water surface transmittance of light in water. The factors depend not only on the direction of the satellite observation but also on the direction of the incident light. This dependency is called Bidirectional Reflectance Distribution Function (BRDF). Our atmospheric correction process also includes BRDF correction according to Morel and Gentilli (1996), Morel and Gentilli (2002) and Wang (2006).

The BRDF correction term C_{BRDF} in Eq. (3.14) is described as follows.

$$\begin{aligned} nL_w{}^{EX} &= nL_w C_{BRDF} \\ &= nL_w(\lambda, \theta, \theta_0, \Delta\phi)\{(f/Q)_{Eff}(\lambda, \theta, \theta_0, \Delta\phi, \mathrm{IOPs})\} \\ &\quad \left[\frac{\Re_0^{(\mathrm{sun})}(\lambda, \tau_a, W)}{\Re^{(\mathrm{sun})}(\lambda, \theta_0, \tau_a, W)}\right]\left[\frac{\Re_0^{(\mathrm{view})}(\lambda, W)}{\Re^{(\mathrm{view})}(\lambda, \theta, W)}\right], \end{aligned} \tag{10.1}$$

where λ is wavelength, θ is the satellite zenith angle, θ_0 is the solar zenith angle, $\Delta\phi$ is the relative azimuthal angle between the satellite and the sun, τ_a is the optical thickness of the aerosol, W is the wind speed, IOPs is the Inherent Optical Properties, $\{(f/Q)_{Eff}(\lambda, \theta, \theta_0, \Delta\phi, \mathrm{IOPs})\}$ is the BRDF effect of the downward irradiance just beneath the ocean surface and the upward radiance just beneath surface, the ratio of $\Re^{(\mathrm{sun})}$ is the BRDF effect of the downward irradiance from atmosphere to in-water at the air-water interface, $\Re^{(view)}$ is the BRDF effect of the upward radiance from in-water to atmosphere at the air-water interface,. $\Re_0^{(\mathrm{sun})}(\lambda, \tau_a, W)$ is defined for $\Re^{(sun)}(\lambda, \theta_0 = 0, \tau_a, W)$, and $\Re_0^{(\mathrm{view})}(\lambda, W)$ is defined for $\Re^{(\mathrm{view})}(\lambda, \theta = 0, W)$.

In the following sections, we describe each BRDF effect.

10.1 BRDF effect of air-water interface for upward light: $\Re_0^{(\mathrm{view})}/\Re^{(\mathrm{view})}$

The BRDF effect of air-water interface from beneath to above surface $\left[\frac{\Re_0^{(\mathrm{view})}(\lambda, W)}{\Re^{(\mathrm{view})}(\lambda,, \theta, W)}\right]$ in Eq.(10.1) was investigated by Gordon (2005). He found that the effect is negligible for satellite zenith angle θ below 70 degrees, so that it can be easily calculated as the ratio of Fresnel reflectivity f by the following formula,

$$\left[\frac{\Re_0^{(\mathrm{view})}(\lambda, W)}{\Re^{(\mathrm{view})}(\lambda, \theta, W)}\right] = \frac{1 - f(\theta = 0, \lambda)}{1 - f(\theta, \lambda)}. \tag{10.2}$$

See Chapter 8 for the calculation of $f(\theta, \lambda)$.

10.2 BRDF effect of air-water interface for downward light: $\Re_0^{(sun)}/\Re^{(\mathrm{sun})}$

The BRDF effect of air-water interface from above to beneath surface $\left[\frac{\Re_0^{(\mathrm{sun})}(\lambda,\tau_a,W)}{\Re^{(\mathrm{sun})}(\lambda,\theta_0,\tau_a,W)}\right]$ is calculated by Wang(2006). This effect is expressed as a function of λ, τ_a and θ_0, and it can be approximated using the irradiance transmittances across downward the air–water interface ($\overline{t_{df}}$) as follows.

$$\left[\frac{\Re_0^{(sun)}(\lambda, \tau_a, W)}{\Re^{(sun)}(\lambda, \theta_0, \tau_a, W)}\right] \approx \frac{\overline{t_{df}}(\lambda, \theta_0 = 0, \tau_a, W)}{\overline{t_{df}}(\lambda, \theta_0, \tau_a, W)}, \tag{10.3}$$

The irradiance transmittance is defined by the following equation,

$$\overline{t_{df}} = \frac{E_d^{(-)}(\lambda, \theta_0, \tau_a, W)}{E_d^{(+)}(\lambda, \theta_0, \tau_a, W)}, \tag{10.4}$$

where $E_d^{(-)}(\lambda, \theta_0, \tau_a, W)$ and $E_d^{(+)}(\lambda, \theta_0, \tau_a, W)$ are downward irradiance just beneath, and just above the surface, respectively.

Wang (2006) found that $\Re^{(sun)}$ ratio in Eq. (10.3) is almost independent of the optical properties of the aerosol, and the ratio is expressed as follows.

$$\left[\frac{\Re_0^{(\mathrm{sun})}(\lambda, \tau_a, W)}{\Re^{(\mathrm{sun})}(\lambda, \theta_0, \tau_a, W)}\right] \approx \mathrm{Corf}^{(\mathrm{Sun})}(\lambda, \theta_0, W) = 1 + \sum_{i=1}^{4} c_i(\lambda, \sigma)[\ln \cos \theta_0], \tag{10.5}$$

$$\sigma = 0.0731 \cdot \sqrt{W}, \tag{10.6}$$

where σ is re-scaled wind speed, W [m/s], and the coefficient $c_i(\lambda, \sigma)$ is shown in Table V.1 in Appendix V. Interpolation of these coefficients is done by bi-linear interpolation for λ and σ.

10.3 BRDF effect of in-water ocean: $\{(f/Q)_{Eff}\}$

BRDF effect of in-water ocean $\{(f/Q)_{Eff}(\lambda,\theta,\theta_0,\Delta\phi,C)\}$ is expressed by Morel and Gentili (2002) as follows.

$$\{(f/Q)_{Eff}(\lambda,\theta,\theta_0,\Delta\phi,\mathrm{IOPs})\} = \left[\frac{f(\lambda,\theta_0=0,\mathrm{IOPs})}{Q(\lambda,\theta_0=0,\theta'=0,\Delta\phi=0,\mathrm{IOP}s)}\right] \Big/ \left[\frac{f(\lambda,\theta_0,\mathrm{IOPs})}{Q(\lambda,\theta_0,\theta',\Delta\phi,\mathrm{IOPs})}\right], \tag{10.7}$$

$$\theta' = \sin^{-1}\frac{\sin\theta}{n(\lambda)}, \tag{10.8}$$

where $\theta^{'}$ is the refractive angle in water corresponding to θ, n is the refractive index of seawater with respect to the wavelength λ, Q is the ratio of the upward irradiance to the downward radiance just beneath ocean surface, and f is the ratio of the upward irradiance to the downward radiance just beneath ocean surface.

The ratio $f(\lambda,\theta_0,\mathrm{IOPs})/Q(\lambda,\theta_0,\theta',\Delta\phi,\mathrm{IOPs})$ is then expressed as,

$$\left[\frac{f(\lambda,\theta_0,\mathrm{IOPs})}{Q(\lambda,\theta_0,\theta',\Delta\phi,\mathrm{IOPs})}\right] = g(\lambda,\theta_0,\theta',\Delta\phi,\mathrm{Chl}), \tag{10.9}$$

where Chl is chlorophyll-a concentration [mg/m^3]. The function g is given as a f/Q lookup table, where we calculate the pixel-wise value with linear interpolation over $\theta_0,\theta',\Delta\phi$ and Chl. See Appendix VI for details of the lookup table.

11. Ancillary data

As ancillary data set, the atmospheric correction refers to the columnar ozone amount, sea surface pressure, and sea surface wind speed data during the pixel-wise processing.

11.1 Ozone content

The amount of ozone is used to evaluate the ozone transmittance. The amount of ozone is expressed in terms of Dobson unit (DU), which is virtual/physical thickness of the columnar ozone under assumed standard condition (1 atm, 0° C) such that 100 DU corresponds to 1 mm of the ozone layer thickness.

The data set comes from the OMI (Ozone Monitoring Instrument) measurement, or TOVS (Advanced Tiros-N Operational Vertical Sounder) measurement.

11.2 Sea Surface Pressure

Sea surface pressure is used to calculate the reflectance and transmission of gas molecules. The data used is the objective analysis data (GGLA) provided by the Japan Meteorological Agency.

11.3 Sea Surface Wind Speed

Sea surface wind speeds are used for correcting sunglitter reflectance, whitecaps, and BRDF. We use the objective analysis data (GGLA) provided by the the Japan Meteorological Agency.

Reference

Ahn, J. H., Park, Y. J., Kim, W., Lee, B., and Oh, I. S. (2015), "Vicarious calibration of the Geostationary Ocean Color Imager," *Optical Express*, Vol.23, pp.23236-23258.

Bodhaine, B. A., N. B. Wood, E. G. Dutton, J. R. Slusser (1999), On Rayleigh Optical Depth Calculations. *J. Atmos. Oceanic Technol.*, Vol.16, pp.1854–1861. doi: 10.1175/1520-0426(1999)016<1854:ORODC>2.0.CO;2

Cox, C., and W. Munk (1954a), Measurement Of The Roughness Of TheSea Surface From Photographs Of The Suns Glitter, *J. Opt. Soc. Am.*, Vol.44, pp.838–850.

Cox, C., and W. Munk (1954b), Statistics of the sea surface derived from sun glitter, *J. Marine Research*, Vol.13, pp.198–227.

Cox, C., and W. Munk (1956), Slopes of the sea surface deduced fromphotographs of sun glitter, *Scripps Institution of Oceanography*.

Frouin, R., M. Schwindling and P.-Y. Deschamps (1996), Spectral reflectance of sea foam in the visible and near-infrared: In situ measurements and remote sensing implications, *J. Geophysical Research*, Vol. 101, No.C6, pp14,361-14,371.

Fukushima, H., A. Higurashi, Y. Mitomi, T. Nakajima, T. Noguchi, T. Tanaka and M. Toratani (1998), Correction of atmospheric effect on ADEOS/OCTS ocean color data: Algorithm description and evaluation of its performance, *J. Oceanography*, Vol.54, pp.417-430.

Gordon H. R. (1997), Atmospheric correction of ocean color imagery in the Earth Observing System era, *J. Geophysical Research*, Vol. 102, No. D14, pp. 17,081-17,106, Gordon, H. R., J.W. Brown, and R. H. Evans (1988), Exact Rayleigh scattering calculations for use with the Nimbus-7 Coastal Zone Color Scanner, *Applied Optics*, Vol.27, pp.862-871.

Gordon H. R. and M. Wang (1994), Retrieval of water-leaving radiance and aerosol optical thickness over the oceans with SeaWIFS: a preliminary algorithm, *Applied Optics*, Vol.33, pp.443–452.

Lee, Z. P., Kendall L. Carder, and Robert A. Arnone (2002), Deriving inherent optical properties from water color: a multiband quasi-analytical algorithm for optically deep waters, *Applied Optics*, Vol.41, 5755-5772.

Morel, A., D. Antoine, and B. Gentili (2002), Bidirectional reflectance of oceanic waters: acconting for Raman emission and varying particle scattering phase function, *Applied Optics*, Vol.41, No..30, pp.6289-6306.

Mobley, C. D., J. Werdell, B. Franz, Z. Ahmad and S. Bailey (2016), Atmospheric Correction for Satellite Ocean Color Radiometry, *NASA Technical Memorandum*, 2016-217551, p.85.

Morel, A. and B. Gentili (1996), Diffuse reflectance of oceanic waters. III. Implication of bidirectionality for the remote sensing problem, *Applied Optics*, Vol. 35, pp.4850-4862.

Ota, Y., A. Higurashi, T. Nakajima and T. Yokota (2010), Matrix formulations of radiative transfer including the polarization effect in a coupled atmosphere-ocean system, *J. Quantitative Spectroscopy and Radiative Transfer*, Vol.111, pp.878–894.

Stramska, M. and T. Petelski (2003), Observations of oceanic whitecaps in the north polar waters of the Atlantic, *J. Geophysical Research*, Vol.108, No.C3, 3086. doi: 10.1029/2002JC001321

Tanaka, A., M. Kishino, R. Doerffer, H. Schiller, T. Oishi and T. Kubota (2004), Development of a Neural Network Algorithm for Retrieving Concentrations of Chlorophyll, Suspended Matter and Yellow Substance from Radiance Data of the

Ocean Color and Temperature Scanner, *J. Oceanography*, Vol.60, pp.519–530.

Toratani, M., H. Fukushima, H. Murakami and A. Tanaka (2007), Atmospheric correction scheme for GLI with absorptive aerosol correction, *J. Oceanography*, Vol.63, pp. 525-532.

Voigt, S., J. Orphal, K. Bogumil, J. P. Burrows (2001), The temperature dependence (203-293K) of the absorption cross sections of O3 in the 230-850 nm region measured by Fourier-transform spectroscopy, *J. Photochemistry and Photobiology A: Chemistry*, Vol. 143.

Wang, M. and Bailey, S. W. (2001), Correction of sun glint contamination on the SeaWiFS ocean and atmosphere products, *Applied Optics*, Vol.40, pp.4790-4798.

Wang, M. (2006), Effects of ocean surface reflectance variation with solar elevation on normalized water-leaving radiance, *Applied Optics*, Vol.45, pp.4122-4128.

Appendix I Mean extraterrestrial solar irradiance

Table I.1 and Table I.2 show the solar irradiance for the GCOM-C/SGLI bands (JAXA/EORC, 2010), The SGLI ocean color atmospheric correction process refers to the solar irradiance at center wavelength for each channel of the nadir-looking instrument, to take the irradiance as the mean solar irradiance ($\overline{F_0}$) .

Table I.1 Solar Irradiance of GCOM-C/SGLI on Visible and Near-Infrared (VNR)

Band	Telescope	Center wavelength: λ_c [nm]	Solar irradiance: F_0 [$Wm^{-2}\mu m^{-1}$]
VNR01	Left	379.853	1093.5379
VNR02		412.306	1711.2835
VNR03		443.443	1903.2471
VNR04		489.686	1937.9540
VNR05		529.638	1850.9682
VNR06		565.926	1797.4827
VNR07		672.002	1502.5522
VNR08		672.148	1502.1799
VNR09		762.917	1245.8937
VNR10		866.023	956.2896
VNR11		867.023	956.5311
VNR01	Nadir	380.030	1092.1436
VNR02		412.514	1712.1531
VNR03		443.240	1898.3185
VNR04		489.849	1938.4602
VNR05		529.640	1850.9604
VNR06		566.155	1797.1344
VNR07		671.996	1502.5667
VNR08		672.098	1502.3177
VNR09		763.074	1245.3663
VNR10		866.765	956.2323
VNR11		867.120	956.5352
VNR01	Right	380.212	1090.5931
VNR02		412.589	1712.4760
VNR03		443.051	1893.5879
VNR04		490.311	1941.0715

VNR05	529.664	1851.0657
VNR06	566.377	1796.8275
VNR07	671.950	1502.6962
VNR08	672.120	1502.2582
VNR09	763.234	1244.8290
VNR10	866.713	956.2577
VNR11	867.086	956.5735

SGLI/VNR has three telescopes (Left, Nadir and Right).

Table I.2 Solar Irradiance of GCOM-C/SGLI on Short Wave Infrared (SWI)

Band	Center wavelength: λ_c [nm]	Solar irradiance: F_0 [$Wm^{-2}\mu m^{-1}$]
SWI01	1054.994	646.5213
SWI02	1385.351	361.2250
SWI03	1634.506	237.5784
SWI04	2209.481	84.2413

Appendix II. Ratio of aerosol Extinction Coefficient (K_{ext}) for Aerosol Models

The spectral dependency of the aerosol extinction coefficient K_{ext} is an important characteristics of different aerosol type. The atmospheric correction uses the spectral ratio of K_{ext} to determine the most likely aerosol model pair. The spectral ratio is also used to determine the AOT and aerosol reflectance at each visible band. The model-specific spectral ratio of K_{ext} is tabulated as a look-up table, which is referenced during the atmospheric correction process. The contents of the LUT is showin in Table II.1. Note that K_{ext} values are normalized with K_{ext} at VN10 band because we only need their "relative" value. Fig. II.1 shows the spectral dependency for all the nine aerosol models.

Table II.1. K_{ext} LUT

Model	VN1	VN2	VN3	VN4	VN5	VN6	VN7	VN9	VN10	SW1	SW2	SW3	SW4
1	2.976	2.750	2.554	2.285	2.081	1.914	1.514	1.240	1.000	0.714	0.393	0.260	0.085
2	2.599	2.417	2.259	2.042	1.877	1.742	1.418	1.196	1.000	0.764	0.494	0.376	0.209
3	2.340	2.188	2.056	1.874	1.737	1.624	1.352	1.166	1.000	0.799	0.563	0.455	0.294
4	2.007	1.893	1.795	1.659	1.556	1.472	1.268	1.126	1.000	0.843	0.652	0.558	0.403
5	1.758	1.674	1.600	1.499	1.422	1.359	1.205	1.098	1.000	0.870	0.710	0.624	0.475
6	1.548	1.487	1.434	1.361	1.306	1.260	1.149	1.071	1.000	0.908	0.785	0.713	0.575
7	1.379	1.338	1.303	1.253	1.216	1.185	1.108	1.053	1.000	0.927	0.821	0.751	0.610
8	1.184	1.166	1.150	1.128	1.111	1.096	1.059	1.030	1.000	0.953	0.873	0.811	0.674
8	0.914	0.923	0.932	0.944	0.953	0.961	0.979	0.991	1.000	1.007	0.997	0.974	0.889

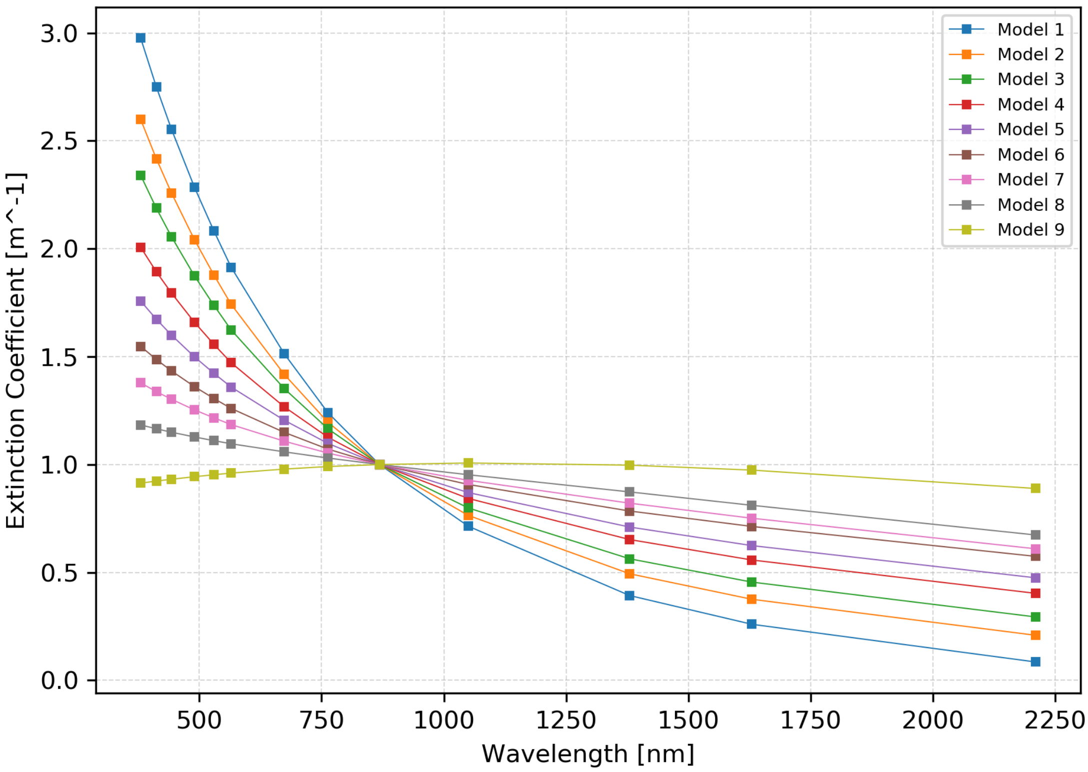

Figure II.1. K_{ext} values normalized by K_{ext} at VN10 for each assumed aerosol model. Solid lines represent LUT values which is band weighted averaged.

Appendix III. Single Scattering Albedo(ω_A) for Aerosol Models

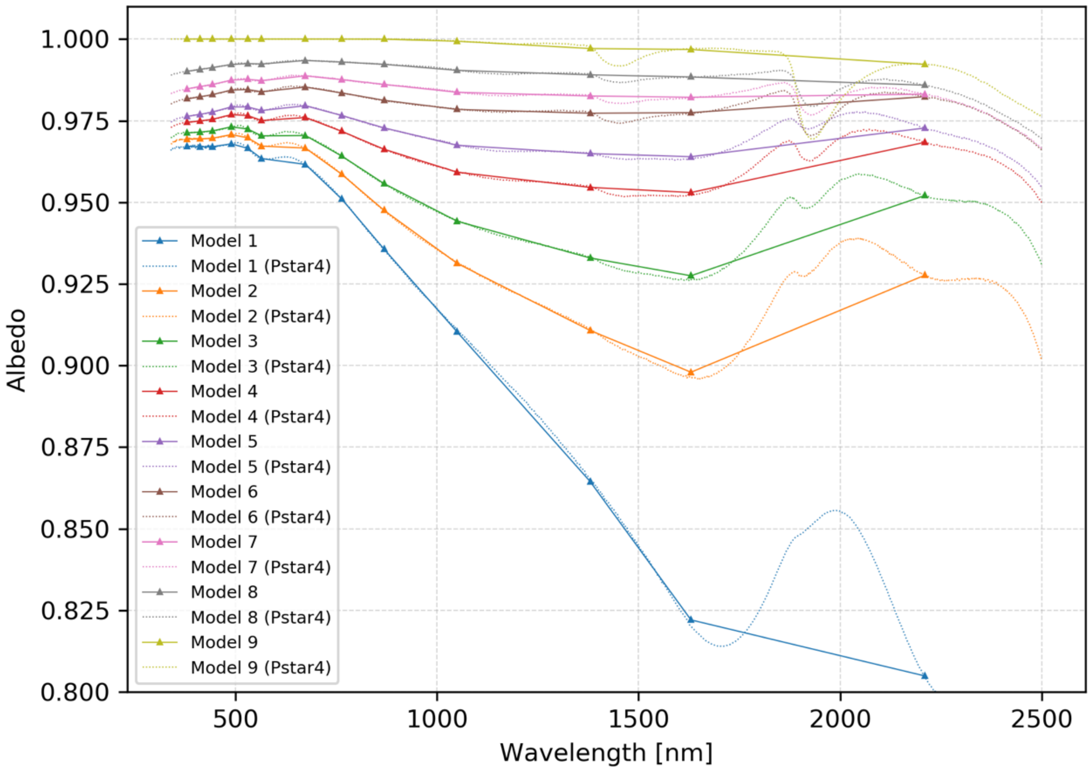

Figure III.1. SSA for each assumed aerosol model. Solid lines represent LUT values which is band weighted averaged. Dash lines represent raw values calculated by Pstar4.

Table III.1. ω_A LUT

Model	VN1	VN2	VN3	VN4	VN5	VN6	VN7	VN9	VN10	SW1	SW2	SW3	SW4
1	0.9672	0.9670	0.9670	0.9679	0.9665	0.9634	0.9616	0.9511	0.9357	0.9103	0.8644	0.8221	0.8049
2	0.9694	0.9694	0.9696	0.9707	0.9698	0.9672	0.9666	0.9586	0.9475	0.9313	0.9107	0.8980	0.9277
3	0.9713	0.9715	0.9719	0.9731	0.9724	0.9703	0.9705	0.9642	0.9557	0.9442	0.9329	0.9275	0.9521
4	0.9745	0.9749	0.9754	0.9768	0.9766	0.9751	0.9760	0.9718	0.9662	0.9592	0.9546	0.9530	0.9684
5	0.9763	0.9769	0.9776	0.9792	0.9792	0.9781	0.9796	0.9766	0.9728	0.9675	0.9649	0.9640	0.9727
6	0.9817	0.9823	0.9830	0.9844	0.9845	0.9839	0.9853	0.9835	0.9812	0.9784	0.9773	0.9775	0.9823
7	0.9847	0.9854	0.9861	0.9874	0.9877	0.9873	0.9887	0.9876	0.9861	0.9837	0.9826	0.9822	0.9831
8	0.9901	0.9907	0.9913	0.9922	0.9925	0.9924	0.9935	0.9930	0.9923	0.9904	0.9890	0.9884	0.9859
8	0.9859	1.0000	1.0000	1.0000	1.0000	1.0000	0.9859	1.0000	1.0000	0.9993	0.9971	0.9968	0.9859

Appendix IV. QA Flags and Masks

Table IV.1 QA flag and masks

Bit	Name	Description	Criterion	Mask
0	DATAMISS	No observation data in one or more band[s]		L2
1	LAND	Land pixel		L2
2	ATMFAIL	Atmospheric correction failure		L2
3	CLDICE	Apparent cloud/ice (high reflectance)	$\rho_A>0.04$	L2
4	CLDAFFCTD	Cloud-affected (near-cloud or thin/sub-pixel cloud)	$\rho_A>0.03$	L3
5	STRAYLIGHT	Stray light anticipated (ref. L1B stray light flags & image)		
6	HIGLITN	High sun glint predicted (atmospheric corr. abandoned)	$[\rho_G]_N > 0.02$	L2
7	MODGLINT	High sun glint predicted (atmospheric corr. abandoned)	$[\rho_G]_N > 0.005$	L3
8	HIOSOLZ	Solar zenith larger than threshold	$\theta_0 > 70°$	L3
9	HITAUA	Aerosol optical thickness larger than threshold	$\tau_A > 0.5$	
10	GAMMA-OUT	Atmospheric correction warning: Gamma out-of-bounds		
11	OVERITER	Maximum iterations reached for NIR correction		
12	NEGNLW	Negative nLw in one or more bands		
13	HIGHWS	Surface wind speed higher than threshold	W/S > 12m/s	
14	ATM-METHOD	NIR atmospheric correction: 0, SWIR atmospheric correction: 1		
15	SPARE	Spare		

Appendix V. Look-up Table for BRDF Correction function $\mathbf{Corf}^{(\mathrm{Sun})}$

Table V.1 Coefficients c_1, c_2, c_3, c_4 from Wang (2006)

Wind speed: W (m/s)	σ	c_i	Wavelengths: λ(nm)					
			412	443	490	510	555	670
0	0.000	c_1	-0.0087	-0.0122	-0.0156	-0.0163	-0.0172	-0.0172
		c_2	0.0638,	0.0415	0.0188	0.0133	0.0048	-0.0003
		c_3	-0.0379	-0.0780	-0.1156	-0.1244	-0.1368	-0.1430
		c_4	-0.0311	-0.0427	-0.0511	-0.0523	-0.0526	-0.0478
1.9	0.100	c_1	-0.0011	-0.0037	-0.0068	-0.0077	-0.0090	-0.0106
		c_2	0.0926	0.0746	0.0534	0.0473	0.0368	0.0237
		c_3	-5.3E-4	-0.0371	-0.0762	-0.0869	-0.1048	-0.1260
		c_4	-0.0205	-0.0325	-0.0438	-0.0465	-0.0506	-0.0541
7.5	0.200	c_1	6.8E-5	-0.0018	-0.0011	-0.0012	-0.0015	-0.0013
		c_2	0.1150	0.1115	0.1075	0.1064	0.1044	0.1029
		c_3	0.0649	0.0379	0.0342	0.0301	0.0232	0.0158
		c_4	0.0065	-0.0039	-0.0036	-0.0047	-0.0062	-0.0072
16.9	0.300	c_1	-0.0088	-0.0097	-0.0104	-0.0106	-0.0110	-0.0111
		c_2	0.0697	0.0678	0.0657	0.0651	0.0640	0.0637
		c_3	0.0424	0.0328	0.0233	0.0208	0.0166	0.0125
		c_4	0.0047	0.0013	-0.0016	-0.0022	-0.0031	-0.0036
30.0	0.400	c_1	-0.0081	-0.0089	-0.0096	-0.0098	-0.0101	-0.0104
		c_2	0.0482	0.0466	0.0450	0.0444	0.0439	0.0434
		c_3	0.0290	0.0220	0.0150	0.0131	0.0103	0.0070
		c_4	0.0029	0.0004	-0.0017	-0.0022	-0.0029	-0.0033

Appendix VI. Look-Up Table of f over Q

The table “morel_fq.nc” is available in DISTRIB_fQ_with_Raman.tar.gz which can be downloaded from the Web site ftp://oceane.obs-vlfr.fr/pub/gentili/AppliedOptics2002/.

The structure of table (morel_fq.nc) is as follows.

- Wavelengths: 412.5, 442.5, 490, 510, 560, 620, and 660 nm (7 wavelengths) (MERIS wavelengths)
- CHL: 0.03, 0.1, 0.3, 1.0, 3.0, 10.0 mg/m^3 (6 levels) (approximately equally spaced on log-scale)
- Solar zenith angle: 0, 15, 30, 45, 60, 75 degrees (6 levels)
- Satellite zenith angles: 1.078, 3.411, 6.289, 9.278, 12.3, 15.33, 18 .37, 21.41, 24.45, 27.5, 30.54, 33.59, 36.64, 39. 69, 42.73, 45.78, 48.83° (17 steps)
- Relative azimuth: 0, 15, 30, 45, 60, 75, 90, 105, 120, 135, 150, 165, 180° (13 levels)

This table was created for MERIS. For SGLI atmospheric correction, the closest wavelength is chosen for lookup.